

# Promoting Energy Transfer via Manipulation of Crystallization Kinetics of Quasi-2D Perovskites for Efficient Green Light-Emitting Diodes

**Citation for published version (APA):**

Guo, Z., Zhang, Y., Wang, B., Wang, L., Zhou, N., Qiu, Z., Li, N., Chen, Y., Zhu, C., Xie, H., Song, T., Song, L., Xue, H., Tao, S., Chen, Q., Xing, G., Xiao, L., Liu, Z., & Zhou, H. (2021). Promoting Energy Transfer via Manipulation of Crystallization Kinetics of Quasi-2D Perovskites for Efficient Green Light-Emitting Diodes. *Advanced Materials*, 33(40), Article 2102246. Advance online publication. <https://doi.org/10.1002/adma.202102246>

**Document license:**  
TAVERNE

**DOI:**  
[10.1002/adma.202102246](https://doi.org/10.1002/adma.202102246)

**Document status and date:**  
Published: 07/10/2021

**Document Version:**  
Publisher's PDF, also known as Version of Record (includes final page, issue and volume numbers)

**Please check the document version of this publication:**

- A submitted manuscript is the version of the article upon submission and before peer-review. There can be important differences between the submitted version and the official published version of record. People interested in the research are advised to contact the author for the final version of the publication, or visit the DOI to the publisher's website.
- The final author version and the galley proof are versions of the publication after peer review.
- The final published version features the final layout of the paper including the volume, issue and page numbers.

[Link to publication](#)

**General rights**

Copyright and moral rights for the publications made accessible in the public portal are retained by the authors and/or other copyright owners and it is a condition of accessing publications that users recognise and abide by the legal requirements associated with these rights.

- Users may download and print one copy of any publication from the public portal for the purpose of private study or research.
- You may not further distribute the material or use it for any profit-making activity or commercial gain
- You may freely distribute the URL identifying the publication in the public portal.

If the publication is distributed under the terms of Article 25fa of the Dutch Copyright Act, indicated by the "Taverne" license above, please follow below link for the End User Agreement:

[www.tue.nl/taverne](http://www.tue.nl/taverne)

**Take down policy**

If you believe that this document breaches copyright please contact us at:

[openaccess@tue.nl](mailto:openaccess@tue.nl)

providing details and we will investigate your claim.

# Promoting Energy Transfer via Manipulation of Crystallization Kinetics of Quasi-2D Perovskites for Efficient Green Light-Emitting Diodes

Zhenyu Guo, Yu Zhang, Bingzhe Wang, Liding Wang, Ning Zhou, Zhiwen Qiu, Nengxu Li, Yihua Chen, Cheng Zhu, Haipeng Xie, Tinglu Song, Lei Song, Haibo Xue, Shuxia Tao, Qi Chen, Guichuan Xing, Lixin Xiao, Zhiwei Liu, and Huanping Zhou\*

Quasi-2D (Q-2D) perovskites are promising materials applied in light-emitting diodes (LEDs) due to their high exciton binding energy and quantum confinement effects. However, Q-2D perovskites feature a multiphase structure with abundant grain boundaries and interfaces, leading to nonradiative loss during the energy-transfer process. Here, a more efficient energy transfer in Q-2D perovskites is achieved by manipulating the crystallization kinetics of different-*n* phases. A series of alkali-metal bromides is utilized to manipulate the nucleation and growth of Q-2D perovskites, which is likely associated with the Coulomb interaction between alkali-metal ions and the negatively charged  $\text{PbBr}_6^{4-}$  frames. The incorporation of  $\text{K}^+$  is found to restrict the nucleation of high-*n* phases and allows the subsequent growth of low-*n* phases, contributing to a spatially more homogeneous distribution of different-*n* phases and promoted energy transfer. As a result, highly efficient green Q-2D perovskites LEDs with a champion EQE of 18.15% and a maximum brightness of 25 800  $\text{cd m}^{-2}$  are achieved. The findings affirm a novel method to optimize the performance of Q-2D perovskite LEDs.


## 1. Introduction

Metal halide perovskites are an emerging family of materials for light-emitting application owing to their high tolerance of defects, high color purity (narrow full-width at half-maximum of emission peak), tunable bandgap, and solution processibility.<sup>[1–5]</sup> The external quantum efficiency (EQE) of green and near-infrared perovskite light-emitting diodes (PeLEDs) has exceeded 20%, suggesting their great potential toward commercialization.<sup>[6–9]</sup> However, in typical 3D perovskite, the low exciton binding energy and long carrier diffusion length make non-radiative recombination outcompete radiative recombination, especially at low exciting density, limiting the electroluminescence efficiency.<sup>[10]</sup> Contrary to 3D perovskite, quasi 2D (Q-2D) perovskites feature higher

Z. Guo, Y. Zhang, N. Zhou, Dr. Z. Qiu, N. Li, Y. Chen, Prof. H. Zhou  
Key Laboratory of Polymer Chemistry and Physics of Ministry of Education  
Beijing Key Laboratory for Theory and Technology of Advanced Battery Materials  
School of Materials Science and Engineering  
Peking University  
Beijing 100871, China  
E-mail: happy\_zhou@pku.edu.cn

B. Wang, Prof. G. Xing  
Joint Key Laboratory of the Ministry of Education  
Institute of Applied Physics and Materials Engineering  
University of Macau  
Macau 999078, China

L. Wang, Prof. Z. Liu  
Beijing National Laboratory for Molecular Sciences (BNLMS)  
State Key Laboratory of Rare Earth Materials Chemistry and Applications  
Beijing Engineering Technology Research Centre of Active Display  
College of Chemistry and Molecular Engineering  
Peking University  
Beijing 100871, China

 The ORCID identification number(s) for the author(s) of this article can be found under <https://doi.org/10.1002/adma.202102246>.

DOI: 10.1002/adma.202102246

C. Zhu, Prof. Q. Chen  
Beijing Key Laboratory of Nanophotonics and Ultrafine Optoelectronic Systems  
School of Materials Science & Engineering  
Beijing Institute of Technology  
Beijing 100081, China

H. Xie  
Hunan Key Laboratory for Super-Microstructure and Ultrafast Process  
College of Physics and Electronics  
Central South University  
Changsha 410083, China

T. Song  
Experimental Center of Advanced Materials  
School of Materials Science & Engineering  
Beijing Institute of Technology  
Beijing 100081, China

Dr. L. Song, H. Xue, Prof. S. Tao  
Materials Simulation and Modelling  
Department of Applied Physics  
Eindhoven University of Technology  
P.O. Box 513, Eindhoven, MB 5600, the Netherlands

Dr. L. Song, H. Xue, Prof. S. Tao  
Center for Computational Energy Research  
Department of Applied Physics  
Eindhoven University of Technology  
P.O. Box 513, Eindhoven, MB 5600, the Netherlands

exciton binding energy and more efficient radiative recombination due to quantum confinement and dielectric confinement effects, exhibiting superior luminescent properties.<sup>[11–13]</sup> Thus, it is of great potential and necessity to develop highly efficient PeLEDs based on Q-2D perovskites.

In Q-2D perovskites, large cations, which cannot enter the lead halogen inorganic framework, are introduced as spacer layers to restrict the growth of grains and confine carriers within smaller domains.<sup>[12,14,15]</sup> Although confinement effects facilitate the radiative recombination, decreased grain sizes would lead to abundant grain boundaries and interfacial defects.<sup>[16,17]</sup> Furthermore, Q-2D perovskites feature multiphase structure with a wide distribution of quantum well widths.<sup>[12,18]</sup> Energy transfer mechanism has been demonstrated to concentrate energy into the narrow bandgap phases in such multiphase structure, but inefficient energy pathways among different phases will lower the energy transfer efficiency and result in deteriorated luminescent properties. Substantial efforts have been taken to diminish the nonradiative loss and boost the luminescent efficiency of Q-2D perovskites by optimizing the distribution of different-*n* phases. For example, composition engineering on the stoichiometry between spacer cation and lead halogen framework was employed in the Q-2D perovskites to achieve a graded energy landscape, which is vital for realizing high photoluminescence quantum yield (PLQY).<sup>[16,17]</sup> Meanwhile, mixing spacer cations was developed to suppress the formation of undesired low-*n* phases, which is detrimental to radiative recombination.<sup>[18–22]</sup> Besides, additives such as methane sulfonate (MeS)<sup>[23]</sup> and L-Norvaline<sup>[24]</sup> are introduced to change the crystallization kinetics for desired distribution of different *n*-phases with enhanced energy transfer. In addition to the quantitative distribution, the spatial distribution of different-*n* phases does also matter, namely the distance between low-*n* and high-*n* phases will influence the energy transfer rate.<sup>[10,25]</sup> Recently, a bifunctional additive of 4-(2-aminoethyl) benzoic acid (ABA) cation was introduced into Q-2D perovskites to diminish the weak van der Waals gaps between individual perovskite layers, realizing promoted coupling of different phases and a more efficient energy transfer.<sup>[26]</sup> These findings suggest that the nonradiative loss during the transfer process is conspicuous and is extremely sensitive to the distribution of the multiphase structure. Although the phase distribution can be optimized by adjusting the precursor composition and processing conditions, the underlying mechanism is closely related to the crystallization kinetics and has yet to be understood. Consequently, the manipulation of crystallization kinetics in Q-2D perovskites is important for accelerating the energy transfer kinetics from low-*n* to high-*n* phases and realizing highly efficient Q-2D PeLEDs.

In this manuscript, we manipulate the crystallization kinetics of the Q-2D perovskite films with the composition of PEA<sub>2</sub>(FAPbBr<sub>3</sub>)<sub>*n*-1</sub>PbBr<sub>4</sub> (*n* = 3) (PEA = phenylethylamine,

FA = formamidine) through the addition of a series of alkali-metal bromides, which is related to the Coulomb interaction between alkali-metal ions and the negatively charged PbBr<sub>6</sub><sup>4-</sup> frames. The addition of KBr is found to restrict the nucleation of high-*n* phases and allow the subsequent growth of low-*n* phases, contributing to a spatially more homogeneous distribution of different-*n* phases and promoted energy transfer. By introducing 50% KBr (molar ratio between KBr and FABr), the modified PEA<sub>2</sub>FA<sub>2</sub>Pb<sub>3</sub>Br<sub>10</sub> film exhibits improved photoluminescence quantum yield (PLQY) of 66.8%. This results in a dramatic boost in EQE of our PeLEDs, delivering a champion EQE of 18.15%, which is among the highest performance in green Q-2D PeLEDs. This work provides a method to accelerate the energy transfer in Q-2D perovskites and improve the efficiency of corresponding PeLEDs through manipulating the nucleation and growth of different-*n* phases.

## 2. Results and Discussion

### 2.1. Impact of Li<sup>+</sup>, Na<sup>+</sup>, K<sup>+</sup> on the Nucleation and Growth of Q-2D Perovskites

Due to the interaction between alkali-metal ions and perovskite,<sup>[27–32]</sup> it is interesting to investigate the influence of alkali-metal halides on the crystallization kinetics of Q-2D perovskites. In order to figure out the effects of alkali-metal ions (Li<sup>+</sup>, Na<sup>+</sup>, K<sup>+</sup>) on the crystallization kinetics of Q-2D perovskites, we analyzed the nucleation and growth process of the corresponding films through a series of characterization (**Figure 1**). The precursor solution was prepared by dissolving an extra amount of alkali-metal bromides with perovskite into dimethyl sulfoxide (DMSO). We denoted different conditions as “w *x*ABr,” where A represents different alkali metals and *x* represent the mole ratio between ABr and FABr. Since the typical one-step crystallization method with chlorobenzene (CB) as antisolvent was employed here (see Experimental section),<sup>[16,33]</sup> we considered that the nucleation was prevailed right after antisolvent dropping before annealing. UV-vis absorption measurements were conducted to study the nucleation states of the precursor films. As shown in Figure 1a and Figure S1 (Supporting Information), different *n*-phases distributions are presented in these films. The pristine film possessed one dominant absorption peak at 432 nm and two obvious absorption signals at 465 and 530 nm, which belong to *n* = 2, 3, and ∞ phase, respectively.<sup>[16,34]</sup> However, for the Li/Na-added films, only two distinct exciton absorption peaks at 400 nm (*n* = 1 phase) and 432 nm emerged. For the K-added film, the absorption signals concentrated on the *n* = 2 and 3 phases, without any signals of the *n* = 1 and higher-*n* phases. Variation of *n*-phases distribution will lead to different luminescence colors.<sup>[18]</sup> As shown in the inset of Figure 1a, the pristine and K-added films emitted green light while the Li/Na-added films emitted deep blue light under ultraviolet lamp excitation. To be noted, as shown in Video S1 (Supporting Information), K-added film also experienced a blue to cyan color change during the CB dropping. Further, we analyzed the condition with equivalent extra PEABr addition (Figure S2, Supporting Information), where the *n*-phases distribution and emitted color of the film are similar as the

Prof. L. Xiao  
State Key Laboratory for Artificial Microstructures and Mesoscopic Physics  
Department of Physics  
Peking University  
Beijing 100871, China

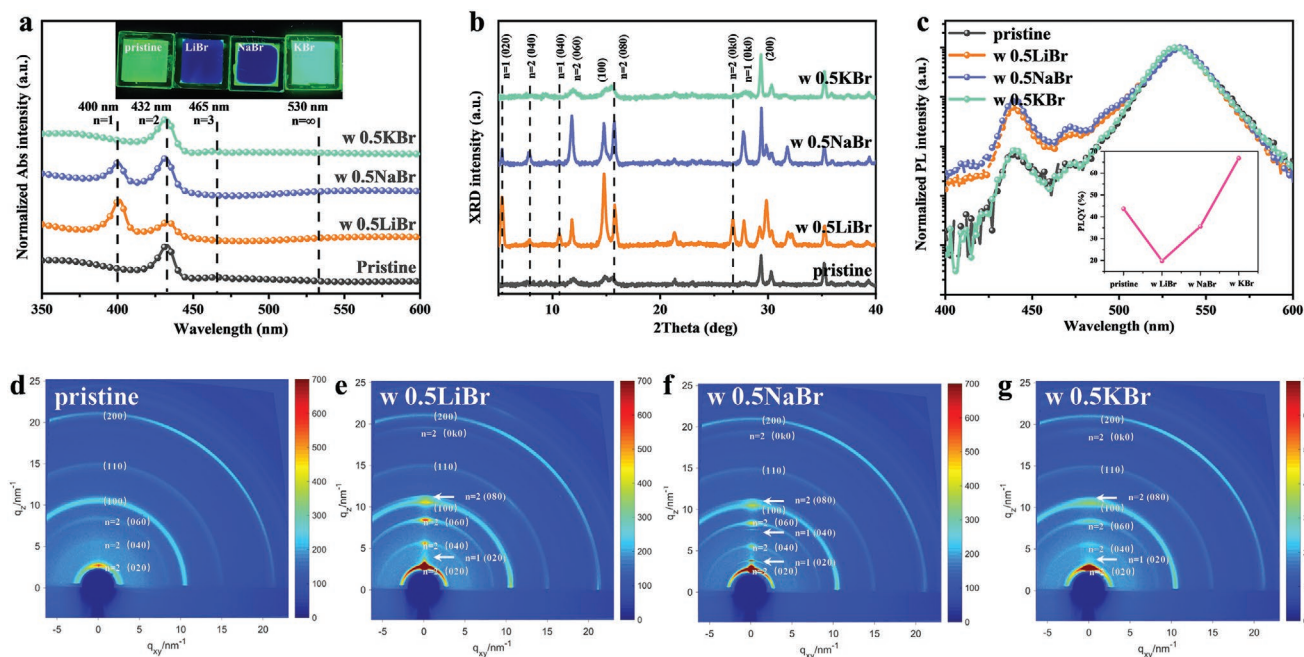


**Figure 1.** Impact of  $\text{Li}^+$ ,  $\text{Na}^+$ ,  $\text{K}^+$  on the nucleation and growth of Q-2D perovskites. a) The absorption spectra of  $\text{PEA}_2(\text{FAPbBr}_3)_2\text{PbBr}_4$  perovskite films right after the antisolvent dropping, with extra addition of LiBr, NaBr, and KBr at the same loading level. The inset shows photoluminescence images of the corresponding perovskite films under ultraviolet lamp excitation. b) XRD patterns. c) PL spectra. d–g) GIWAXS patterns of Q-2D perovskite films after annealing at  $90^\circ\text{C}$  for 60 min with different alkali-metal ions incorporated. The inset of (c) shows the PLQY of the corresponding films. The perovskite films were encapsulated with quartz flakes during the absorption and PL measurements.

Li/Na counterparts. Therefore, we proposed that, compared to the pristine one, the addition of alkali-metal ions can all restrict the nucleation of high- $n$  phases in Q-2D perovskites, contributing to a narrower distribution of  $n$ -phases initially (concentrating on  $n \leq 3$ ).

Thermal annealing process will promote the crystal growth and transform the low- $n$  phases into high- $n$  phases.<sup>[35]</sup> Thus, we performed XRD measurements on the above perovskite films after annealing. As shown in Figure 1b, the peaks at  $14.8^\circ$  and  $29.9^\circ$  belong to (100) and (200) crystallographic planes of high- $n$  phases, respectively, which shows no shift in all samples,<sup>[16,36,37]</sup> indicating alkali-metal ions do not enter the lattice. Besides, there is an appreciable difference in the diffraction peaks and intensity of these films in terms of low- $n$  phases. All the films possess diffraction peaks at  $2\theta$  of  $11.8^\circ$  and  $15.7^\circ$  without shift, indicative of the presence of  $n = 2$  phase<sup>[16]</sup> and that alkali-metal ions do not serve as spacer cations.<sup>[38]</sup> However, in the Li/Na-added films, the relative intensity of  $n = 2$  phase increased dramatically, with two newly formed peaks at  $5.35^\circ$  and  $10.68^\circ$  ( $n = 1$  phase),<sup>[16,38]</sup> when compared to the K-added films. This indicated that K-added films possess similar  $n$ -phases distribution with the pristine film after annealing, while Li/Na-added film exhibited more  $n = 1$  and 2 phases. It is further confirmed by the PL (Figure 1c) and absorption spectra (Figure S3, Supporting Information). PL intensity of the peak at 440 nm ( $n = 2$  phase) in the Li/Na-added films is an order of magnitude higher than that in the pristine and K-added counterparts, in accordance with the increased intensity of exciton absorption peak of  $n = 2$  phase (Figure S3, Supporting Information).<sup>[16,39]</sup> Meanwhile, PLQY (inset of Figure 1c) of the films

differ substantially, which is 43.7%, 19.8%, 35.6% and 66.8% for pristine, Li/Na/K incorporated films, respectively. We attribute the lower PLQY of Li/Na-added films to the less graded energy landscape with more low- $n$  phases, which is consistent with reported works.<sup>[17,19,22]</sup> Thus, the addition of various alkali-metal ions is considered to affect the crystal growing process to a much different extent. Combined with the nucleation with less  $n$ -phases segregation,  $\text{K}^+$  allows the subsequent transformation of  $n = 1, 2$  to higher- $n$  phases in the growing process, which is different from the hindrance of  $\text{Li}^+/\text{Na}^+$  to the transformation.

Grazing-incidence wide-angle X-ray scattering (GIWAXS) measurement was further performed to investigate the crystal phase and crystallinity of the Q-2D films. The detailed analysis of the scattering patterns is listed in Table S1 (Supporting Information). As shown in Figure 1d–g, the scattering ring at  $q = 10.5, 15.1, 21.1 \text{ nm}^{-1}$ , which belongs to the (100), (110), and (200) crystallographic planes of high- $n$  phases, respectively, shows no shift. The scattering rings belonging to (0k0) crystallographic planes of low- $n$  ( $n = 1$  and 2) phases are marked in Figure 1f,g. The integrated intensity of Debye rings versus  $q$  is plotted in Figure S4a,b (Supporting Information), in which stronger intensity of  $n = 2$  phases in Li/Na-added films indicates the formation of more low- $n$  phases, in agreement with the above XRD and PL results. In addition, the presence of Debye–Scherrer rings in Figure 1d indicated a random crystalline orientation in the pristine film. However, the films with  $\text{Li}^+/\text{Na}^+/\text{K}^+$  exhibit stronger scattering spots along the  $q_z$  direction, indicating higher crystallinity and increased crystal orientation, which is clearly shown in the azimuthally integrated GIWAXS intensity plots (Figure S4c,d, Supporting Information).<sup>[40,41]</sup> It

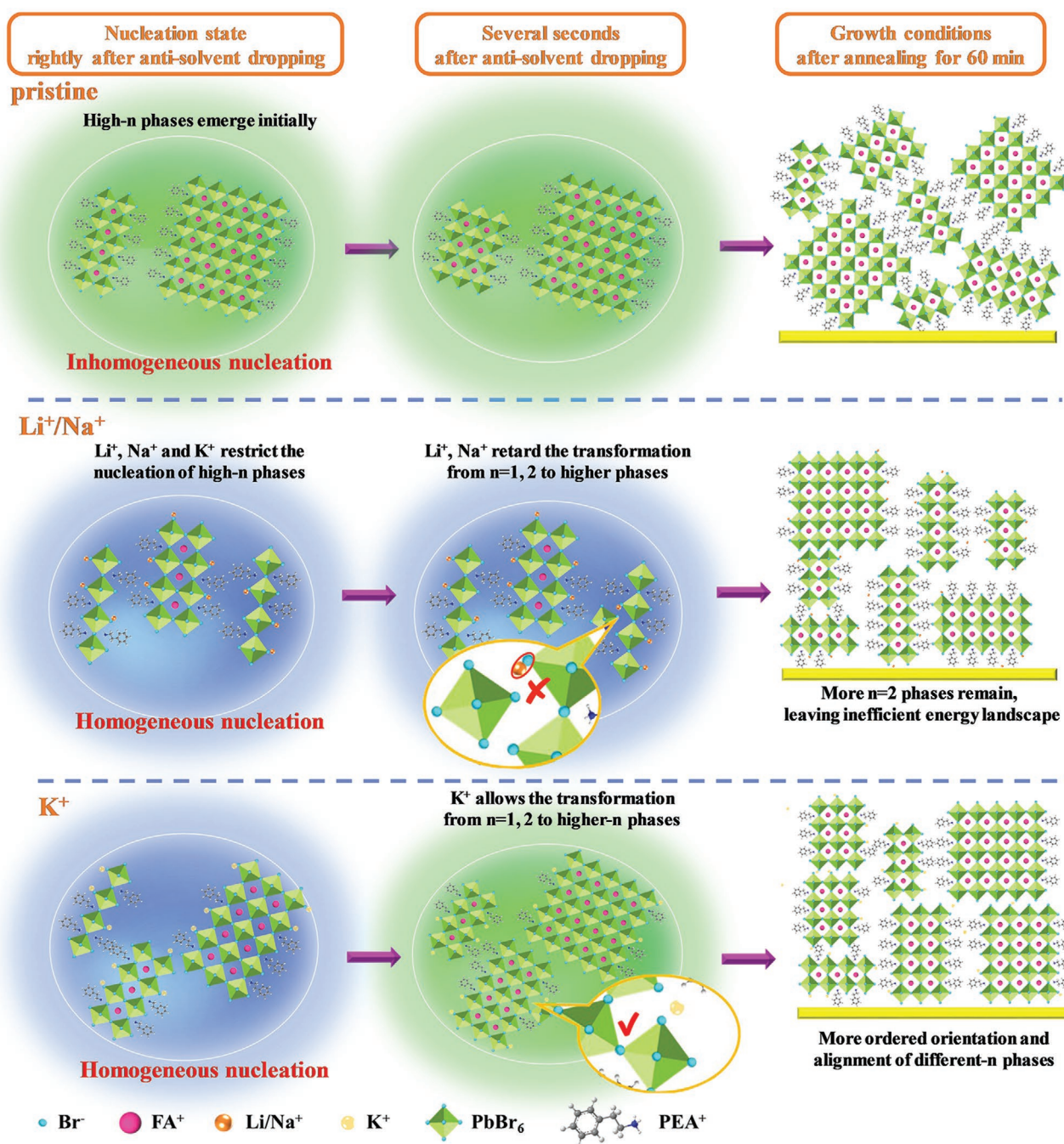


**Figure 2.** Schematic diagram of the impacts of Li<sup>+</sup>, Na<sup>+</sup>, K<sup>+</sup> on the nucleation and growth of Q-2D perovskites.

is believed that the ordered crystal structure is related to the evolution of crystallization kinetics, which is consistent with a previous report that cation cascade doping enables to manipulate the crystal facet orientation due to interfered crystallization kinetics.<sup>[40]</sup>

Based on the above discussion, we illustrated the effects of different alkali-metal ions on the nucleation and growth of Q-2D perovskites in scheme (Figure 2). During the nucleation process (the nucleation is prevailed in the precursor film), the pristine film emits green light because high-*n* phases emerge

initially due to the weak confinement of PEA<sup>+</sup> only. In contrast, addition of Li<sup>+</sup>/Na<sup>+</sup>/K<sup>+</sup> will place extra restriction on the nucleation of high-*n* phases, leaving more low-*n* phases initially and emitting blue light. However, K-added film gradually turns to cyan light several seconds after antisolvent dropping, while Li/Na-added films remain blue. This is also in agreement with the first principle DFT calculations results, that the net atomic charge of nearest halogen surrounding the alkali-metal ions increases by following the order of Li > Na > K (Figures S5 and S6, Supporting Information). It suggests the

enhanced Coulomb interaction between alkali-metal cations and negatively charged  $\text{PbBr}_6^{4-}$ , obeying the trend of  $\text{Li}^+ > \text{Na}^+ > \text{K}^+$  due to their ionic radius difference. The relatively weaker interaction between  $\text{K}^+$  and  $\text{PbBr}_6^{4-}$  frames allows the transformation of low- $n$  to high- $n$  phases, accounting for the emitted cyan light several seconds after antisolvent dropping. Meanwhile, during the growth process (the growth mainly happens during annealing), the stronger interaction between  $\text{Li}^+/\text{Na}^+$  with  $\text{PbBr}_6^{4-}$  frames will prevent more  $\text{PbBr}_6^{4-}$  from entering the lattice and restrict the transformation of low- $n$  phases to high- $n$  phases, resulting in an inefficient energy landscape and deteriorating PL properties. The restriction of  $\text{K}^+$  to growth is weaker and  $n$ -phases distribution in the corresponding films is similar to the pristine films, ensuring efficient energy transfer. In addition, the delayed growth of low- $n$  phases contributes to the higher crystallinity and much-ordered crystal structure in the Li/Na/K-added films.

## 2.2. Characterization of Q-2D Perovskites with KBr Addition

Addition of KBr manipulates the film morphology of Q-2D perovskites, as assessed by scanning electron microscopy (SEM) and atomic force microscopy (AFM) measurements. As seen in Figure 3a, the pristine film possesses full coverage with corrugated structures, which is consistent with previous documents.<sup>[42]</sup> However, the corrugated structures of K-added film become indistinct, showing lower roughness. The root-mean-square (RMS) roughness of the perovskite films across a scanned area of  $10 \times 10 \mu\text{m}^2$  is reduced from 15.73 to 7.43 nm,

as shown in Figure S7 (Supporting Information). To be noted, a few tiny particles are observed on the surface of the films with KBr (Figure S8, Supporting Information). Furthermore, according to the analysis of spatial distribution of  $\text{K}^+$  for the perovskite films by time-of-flight secondary-ion mass spectroscopy (ToF-SIMS) (Figure 3b), the signal intensity of K is appreciable throughout the entire perovskite film and becomes higher at the upper and down interfaces. We can thus conclude that there is adequate  $\text{K}^+$  in the bulk of the perovskite films and the excess  $\text{K}^+$  tend to exist near the upper and down interfaces, which can passivate defects potentially.<sup>[28]</sup>

UV-vis absorption and PL measurements were carried out to investigate the optical properties of  $\text{PEA}_2(\text{FAPbBr}_3)_2\text{PbBr}_4$  films obtained after annealing at  $90^\circ\text{C}$  for 60 min upon the addition of KBr (Figure 3c,d). As shown in Figure 3c, all the four films (KBr:FABr = 0.25, 0.5, 0.75) possess four characteristic absorption signals at 435 nm ( $n = 2$ ), 470 nm ( $n = 3$ ), 490 nm ( $n = 4$ ) and 530 nm ( $n = \infty$ ),<sup>[16,39]</sup> which further confirms KBr has negligible impacts on the distribution of different- $n$  phases. Meanwhile, the PL spectra (Figure 3d) only present single main peak at 530 nm, resulting from the energy transfer from low- $n$  to high- $n$  phases. Normalized PL spectra of these films in logarithmic coordinates shown as dashed lines illustrate that  $n = 2$  and high- $n$  phase are the two main phase in the Q-2D perovskite films. Intriguingly, there is a stepwise augment in the luminescence intensity at higher KBr loading levels, which is consistent with the significantly increased PLQY from 43.7% to 75.4% (Figure 3e). Time-resolved photoluminescence (TRPL) was conducted to analyze the dynamics of carrier recombination. We measured the photoluminescence lifetime of the

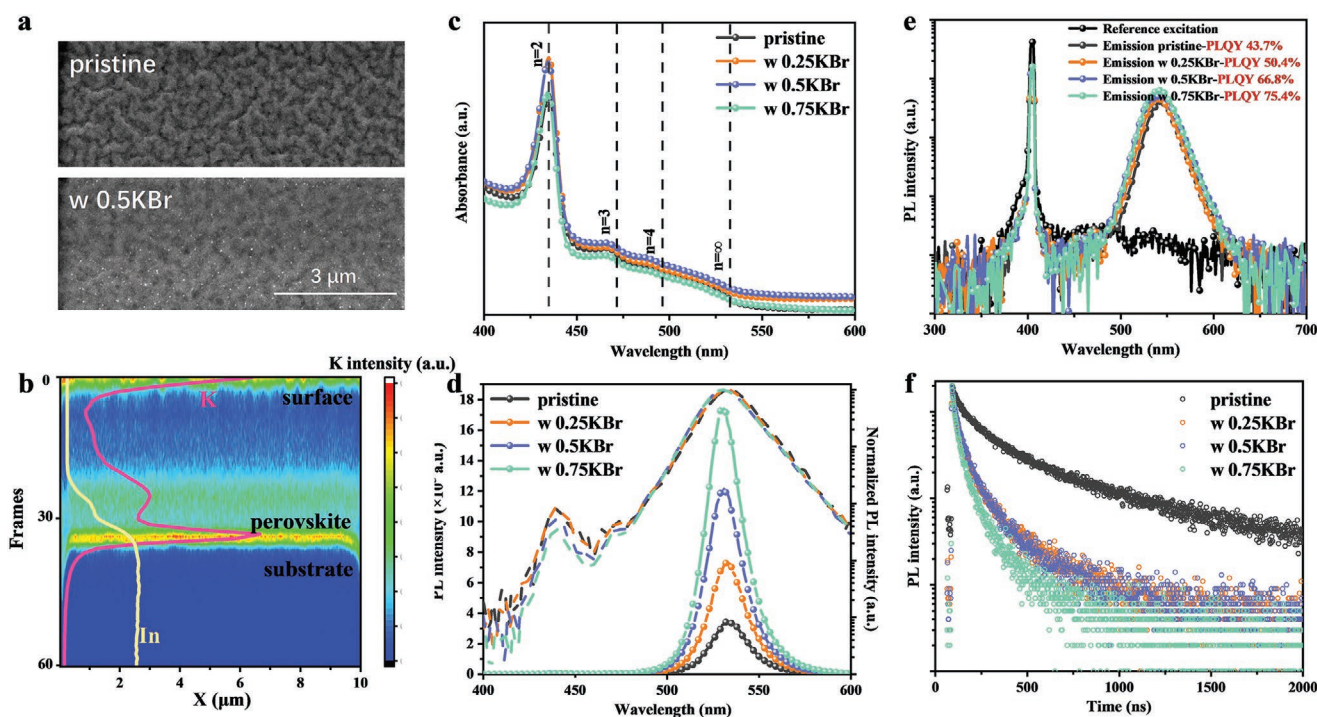


**Figure 3.** Characterization of Q-2D perovskites with KBr addition. a) SEM images of Q-2D perovskite films without and with 0.5KBr-added. b) Cross-sectional mapping of ToF-SIMS signals of  $\text{K}^+$  in the Q-2D perovskite with 0.5KBr-added. c) Absorption spectra, d) PL spectra, e) photoluminescence quantum yield (PLQY), and f) time-resolved photoluminescence (TRPL) of Q-2D perovskite films with different amounts of KBr added.

perovskite films deposited on nonconductive quartz flakes (Figure 3f). The decay of the fluorescence signals was fitted with biexponential rate law and the corresponding lifetimes of the two components are summarized in Table S3 (Supporting Information). We found that the pristine film showed the longest PL lifetime of 291.12 ns, much longer than the K-added films of 81.5, 77.25, and 55.83 ns. Higher PLQY and shorter PL lifetime indicate more effective radiative recombination and accelerated recombination kinetics, respectively, which will be discussed in detail below.

In Q-2D perovskites, the mode and kinetics of recombination are related to the defect density, exciton binding energy, and carrier concentration.<sup>[43]</sup> Addition of extra bromides can afford a bromine-rich environment to potentially eliminate halogen vacancy defects and interact with uncoordinated lead, which is a common strategy to improve the performance of perovskite LEDs.<sup>[7,8,31,33,44,45]</sup> And we propose that KBr has the similar effect as other bromides. X-ray photoelectron spectroscopy (XPS) measurements were performed to examine the interaction between KBr with Pb<sup>2+</sup> and halogen vacancy. As shown in Figure S9 (Supporting Information), the binding energy of Pb 4f<sub>5/2</sub> and Pb 4f<sub>7/2</sub> become smaller after incorporation of KBr, possibly resulting from that Br-rich environments enhance the shielding effect between inner electrons and Pb nucleus.<sup>[26,33]</sup> Furthermore, the passivation of KBr is verified by the TRPL excited by a 505 nm laser, where the excitation wavelength can exclude the effects of energy transfer because low-*n* phases (*n* = 4 phase locating at 490 nm) cannot be excited by the excitation of 505 nm (Figure S10, Supporting Information). Therefore, we propose KBr can passivate defects related to bromine vacancy and the shorter PL lifetime is not attributed to defect-related recombination. Exciton binding energy is a parameter influencing the recombination mode (excitonic or bimolecular recombination) and is related with the recombination rate closely.<sup>[43,46,47]</sup> We measured the exciton binding energy through temperature-dependent PL (Figure S11, Supporting Information).<sup>[31]</sup> Through curve fitting of the integrated PL intensity versus temperature, the binding energy of *n* = ∞ phase is calculated to be 141.9 and 137.5 meV for pristine and K-added film, respectively, showing the negligible change. In Q-2D perovskites, the binding energy between electrons and holes depends on the dielectric confinement effect between the organic spacer layer and inorganic framework.<sup>[12,48]</sup> The unchanged exciton binding energy further indicates that the arrangement between the organic layer and the inorganic layer is not influenced by K<sup>+</sup>. Therefore, we suggest that the enhanced fluorescence emission and shorter carrier lifetime are attributed to changes of carrier concentration in the emitting center, which is closely related to the energy transfer in Q-2D perovskites and will be discussed below in detail.

### 2.3. Energy Transfer Dynamics of Q-2D Perovskite with KBr Addition

Transient absorption (TA) measurements were performed to investigate the energy transfer dynamics in the Q-2D perovskites (Figure 4).<sup>[11,12,26]</sup> There are four photobleaching (PB)

peaks, belonging to *n* = 2, 3, 4, and *n* ≥ 5 phase, respectively, shown in the TA spectra of pristine and K-added perovskites at different timescales (Figure 4a,c), which is in agreement with the absorption spectra (Figure 3c). The intensity evolution of the PB peaks corresponds to the evolution of excited-states populations in the corresponding phases.<sup>[17]</sup> It is observed that the low-*n* phases (*n* = 2, 435 nm) are primarily excited by the pump light within 1 ps, which means the photocarriers are initially formed in low-*n* phases. Within the subsequent 10 ps, the decreased PB peaks of low-*n* phases along with increased bleaching intensity of high-*n* phases (*n* ≥ 5, 523 nm) indicate that the energy transfer from low-*n* to high-*n* phases is quite rapid.<sup>[10]</sup> Addition of KBr will increase the bleaching intensity of *n* = 2 phase at 1 ps, which means the quantity of *n* = 2 phase increase. The phenomenon is related to the retarded growth of low-*n* phases as discussed above, but the increase of *n* = 2 phase is not obvious enough to deteriorate the PL properties of K-added film.

To further study the energy transfer dynamics, we analyzed the evolution of TA signals probed at selected wavelengths corresponding to low-*n* (*n* = 2) phases and high-*n* (*n* ≥ 5) phases as a function of delay time (Figure 4b,d). The evolution of photocarrier populations in a certain phase is associated with the energy transfer process and the recombination behaviors, of which the corresponding timescale differs a lot.<sup>[11,12]</sup> The evolution of each PB intensity can be fitted by a multiexponential function and the fitting parameters are listed in Table S4 (Supporting Information).<sup>[26,49]</sup> In the *n* ≥ 5 phase, the energy transfer and recombination behavior can be described as three processes, among which  $\tau_1$  corresponds to the energy accepting from low-*n* phases,  $\tau_2$  is related to the overlapping of energy accepting and energy decay within *n* ≥ 5 phases (decay dominates in this process),  $\tau_3$  represents all the recombination of exciton in the *n* ≥ 5 phases. As shown in the fitting results, the time constant  $\tau_1$  of K-added film (0.4 ps) is 4.5 times shorter than that in the pristine one (1.8 ps), which indicates that energy transfer into high-*n* phases is realized at a faster rate in K-added film. Faster energy transfer means less energy loss during the transfer process and further higher carrier concentration in the emitting center (high-*n* phases). Higher carrier concentration will induce higher-order recombination process for luminescence (especially bimolecular radiative recombination), consuming carriers at a faster rate, which corresponds to the TRPL results in Figure 3f. The results are in agreement with previously reported carrier density-dependent PL lifetime in Q-2D perovskites.<sup>[24,43]</sup>

Considering the more homogeneous nucleation (less high-*n* phases initially) in K-added film, we suggest that KBr contributes to a more homogeneous distribution of different-*n* phases with less spatial segregation, which accounts for the promoted energy transfer. Meanwhile, restricted nucleation of high-*n* phases enables improved homogeneity of the perovskites film fabricated by one-step method, which is confirmed by the PL spectra of different selected regions shown in Figure S12 (Supporting Information).<sup>[24]</sup> Besides, TA analysis of Li/Na-added films (details in Figure S13 and Table S5, Supporting Information) indicates that more low-*n* phases result in slower energy transfer and severe energy loss, which is consistent with the deteriorated PL emission.

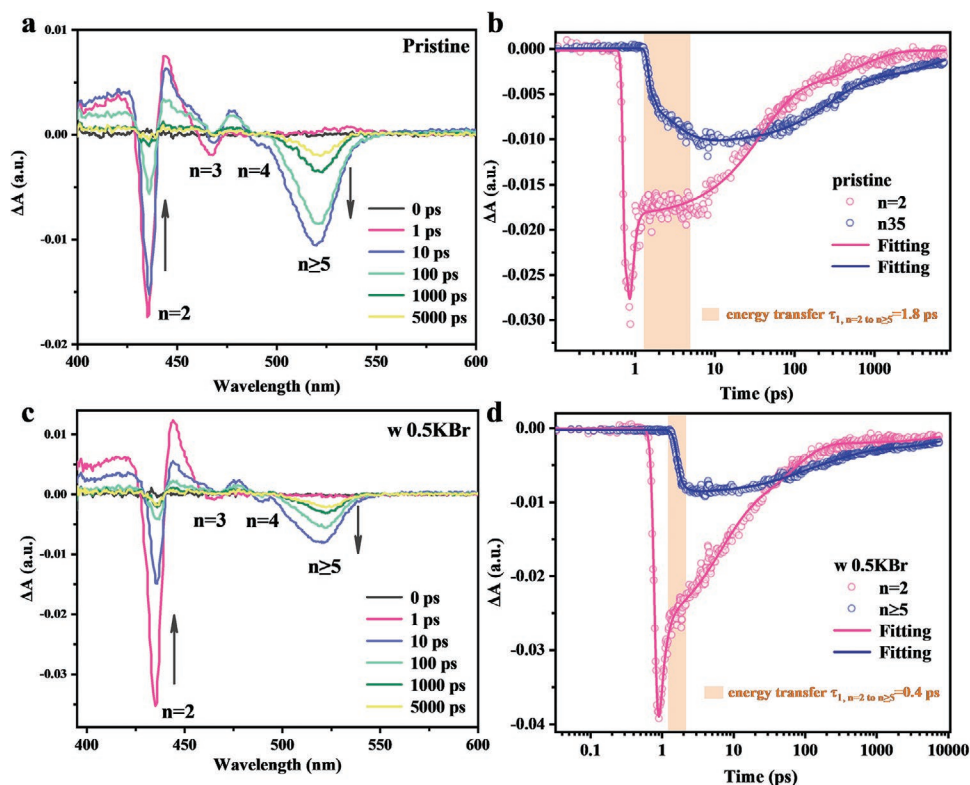


**Figure 4.** Effects of  $K^+$  on the energy transfer process. a,c) Transient absorption spectra at a different probe delay times of pristine (a) and 0.5KBr-added (c) Q-2D perovskite films. b,d) TA kinetics for pristine (b) and 0.5KBr-added (d) Q-2D perovskite films probed at selected wavelengths correspond to  $n = 2$  and  $n \geq 5$  phases as a function of delay time.

#### 2.4. Performance of the Corresponding Q-2D Perovskite LEDs

The addition of moderate KBr could improve the film morphology, reduce trap densities and accelerate the energy transfer, which is expected to improve the performance of perovskite LEDs. Thus, we fabricated the perovskite LEDs with the device structure ITO/PEDOT:PSS/PEA<sub>2</sub>FA<sub>2</sub>Pb<sub>3</sub>Br<sub>10</sub>/TPBi/LiF/Al. Trioctylphosphine oxide (TOPO) is applied as a passivation layer inserted between perovskite film and electron transport layer TPBi, whose validity was confirmed by previous reports.<sup>[16,50,51]</sup> Figure 5a presents the cross-sectional SEM image of the device. The thickness of PEDOT:PSS, Q-2D perovskite layer, TPBi, LiF, and Al electrode are about 25, 100, 40 and 100 nm, respectively. The energy level alignments of each function layer are shown in Figure S14a (Supporting Information), which are extracted from ultraviolet photoelectron spectroscopy (UPS) in Figure S14b (Supporting Information) and the literature.<sup>[16]</sup> It is believed that addition of KBr has no effect on the work function of the perovskites (Figure S14c, Supporting Information). As shown in Figure S15 (Supporting Information), the injection behaviors are further checked by the injection current of hole- and electron-only devices. We fabricated the hole- and electron-only devices with the structure of ITO/PEDOT:PSS/perovskite/MoO<sub>3</sub>/Ag and ITO/SnO<sub>2</sub>/perovskite/TPBi/LiF/Al, respectively. No appreciable difference is observed in the hole and electron current between the pristine and KBr-added devices, indicating the carrier injection is not influenced by KBr. Figure 5b,c are the plots of current efficiency (CE)

versus voltage for LED devices with different alkali-metal ions and different amounts of KBr. The deteriorated PL properties of perovskite with Li<sup>+</sup>/Na<sup>+</sup> certainly result in a drop in the performance of devices. As shown in Figure 5b, the highest CE of the four devices is 46.9 cd A<sup>-1</sup> (pristine), 11.3 cd A<sup>-1</sup> (LiBr), 33.2 cd A<sup>-1</sup> (NaBr), and 57.1 cd A<sup>-1</sup> (KBr). The KBr dramatically boosts the performance of the LED device. Through controlling the content of KBr, we achieved an optimal molar ratio of 0.5 (KBr to FABr). The highest CE is 46.9 cd A<sup>-1</sup> (pristine), 57.8 cd A<sup>-1</sup> (0.25KBr), 78.0 cd A<sup>-1</sup> (0.5KBr), and 65.1 cd A<sup>-1</sup> (0.75KBr). The corresponding champion external quantum efficiency (EQE) of the 0.5KBr-added device reached 18.15%, which is among the highest efficiency of green Q-2D perovskite LEDs. Figure 5d presents the *J*-*V*-*L*-EQE curves of the champion device. The turn-on voltage is below 2.8 V and the highest luminance reaches 25 800 cd m<sup>-2</sup>. Figure 5e is the histogram of maximum EQE measured from 50 devices with 0.5KBr added, showing good reproducibility of our devices. The average EQE is 16.94% with a low relative standard deviation of 2.69%. We also compared the operational stability of our perovskite LEDs at a constant current density of 0.25 mA cm<sup>-2</sup> with an initial luminance (*L*<sub>0</sub>) of approximately 140 cd m<sup>-2</sup>. As shown in Figure 5f, the luminance of the K-added device decayed to half of *L*<sub>0</sub> with a *T*<sub>50</sub> of 59 min, four times longer than the pristine device of 13.5 min. We attribute the improved stability mainly to the passivation effect that reduces ion-migration channels under an external electric field,<sup>[31,50,52-54]</sup> as well as the more efficient energy transfer with less Joule heat.<sup>[55]</sup>



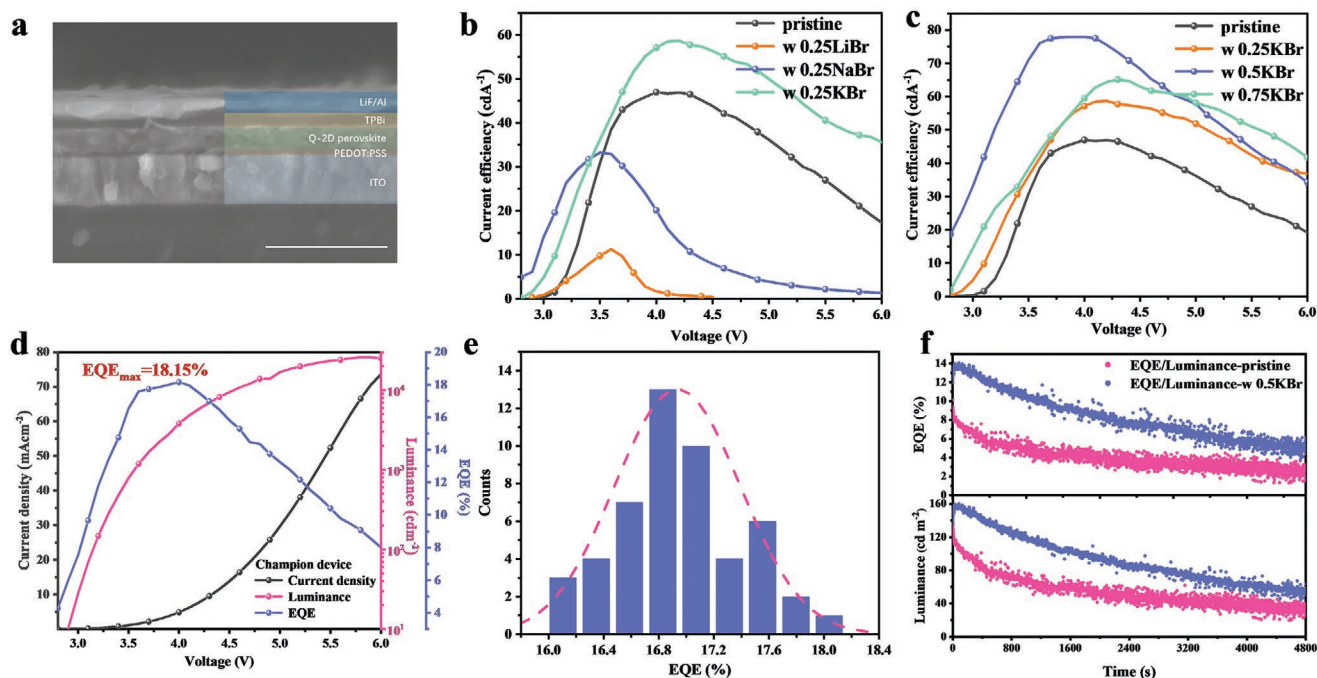


**Figure 5.** Performance of LED devices of Q-2D perovskite. a) Cross-section scanning electron microscopy (SEM) image of the device; scale bar: 500 nm. b,c) Current-efficiency-voltage (CE–V) curves of the Q-2D perovskite LED devices with different alkali-metal ions incorporated (b) and different amounts of KBr incorporated (c). d) *J*–*V*–*L*–EQE curves of the champion device with 0.5KBr added. e) Histogram of maximum EQE measured from 50 devices with 0.5KBr added. f) Stability of the perovskite LED measured at a constant current density of 0.25 mA cm<sup>−2</sup>, with an initial luminance around 140 cd m<sup>−2</sup>.

### 3. Conclusion

We have systematically investigate the effects of alkali-metal ions on the nucleation and growth of Q-2D perovskites, which is likely associated with the strength of Coulomb interaction between alkali-metal ions and the negatively charged PbBr<sub>6</sub><sup>4−</sup> frames. It is demonstrated that the addition of KBr will restrict the nucleation of high-*n* phases and allow the subsequent growth of low-*n* phases. The synergistic manipulation of nucleation and growth contributes to a spatially more homogeneous *n*-phases distribution and promoted energy transfer, along with a more ordered crystal structure. The optimized PEA<sub>2</sub>FA<sub>2</sub>Pb<sub>3</sub>Br<sub>10</sub> film exhibits improved photoluminescence quantum yield (PLQY) of 66.8%. Our corresponding champion device delivers the maximum EQE of 18.15% and the highest luminance of 25 800 cd m<sup>−2</sup>, which is among the highest performance in green Q-2D PeLEDs. This work provides an effective strategy to improve the efficiency of Q-2D PeLEDs from the aspect of manipulating the nucleation and growth of different-*n* phases and accelerating the energy transfer. Our findings further shed light on the understanding of efficient radiative recombination in Q-2D perovskites and emphasize the significance of manipulation of crystallization kinetics.

### 4. Experimental Section

See experimental details in the Supporting Information.

### Supporting Information

Supporting Information is available from the Wiley Online Library or from the author.

### Acknowledgements

This work was supported by the National Key Research and Development Program of China (Grant No. 2017YFA0206701, 2020YFB1506400), and the National Natural Science Foundation of China (Grant No. 51972004), and the Tencent Foundation through the XPLOER PRIZE. The authors thank the engineers of Enlitech for their support during the revision of this work.

### Conflict of Interest

The authors declare no conflict of interest.

### Data Availability Statement

Research data are not shared.

### Keywords

alkali-metal cations, crystallization kinetics, perovskite light-emitting diodes, quasi-2D perovskites

Received: March 23, 2021

Revised: June 21, 2021

Published online: August 15, 2021

- [1] Z. Wei, J. Xing, *J. Phys. Chem. Lett.* **2019**, *10*, 3035.
- [2] W. J. Yin, T. Shi, Y. Yan, *Adv. Mater.* **2014**, *26*, 4653.
- [3] Z.-K. Tan, R. S. Moghaddam, M. L. Lai, P. Docampo, R. Higler, F. Deschler, M. Price, A. Sadhanala, L. M. Pazos, D. Credgington, *Nat. Nanotechnol.* **2014**, *9*, 687.
- [4] M. Worku, A. Ben-Akacha, T. B. Shonde, H. Liu, B. Ma, *Small Sci.* **2021**, *1*, 2000072.
- [5] Y. Zou, L. Cai, T. Song, B. Sun, *Small Sci.* **2021**, *1*, 2000050.
- [6] W. Xu, Q. Hu, S. Bai, C. Bao, Y. Miao, Z. Yuan, T. Borzda, A. J. Barker, E. Tyukalova, Z. Hu, *Nat. Photonics* **2019**, *13*, 418.
- [7] K. Lin, J. Xing, L. N. Quan, F. P. G. de Arquer, X. Gong, J. Lu, L. Xie, W. Zhao, D. Zhang, C. Yan, W. Li, X. Liu, Y. Lu, J. Kirman, E. H. Sargent, Q. Xiong, Z. Wei, *Nature* **2018**, *562*, 245.
- [8] Y. Cao, N. Wang, H. Tian, J. Guo, Y. Wei, H. Chen, Y. Miao, W. Zou, K. Pan, Y. He, H. Cao, Y. Ke, M. Xu, Y. Wang, M. Yang, K. Du, Z. Fu, D. Kong, D. Dai, Y. Jin, G. Li, H. Li, Q. Peng, J. Wang, W. Huang, *Nature* **2018**, *562*, 249.
- [9] Y. Jiang, M. Cui, S. Li, C. Sun, Y. Huang, J. Wei, L. Zhang, M. Lv, C. Qin, Y. Liu, M. Yuan, *Nat. Commun.* **2021**, *12*, 336.
- [10] G. Xing, B. Wu, X. Wu, M. Li, B. Du, Q. Wei, J. Guo, E. K. Yeow, T. C. Sum, W. Huang, *Nat. Commun.* **2017**, *8*, 14558.
- [11] N. Wang, L. Cheng, R. Ge, S. Zhang, Y. Miao, W. Zou, C. Yi, Y. Sun, Y. Cao, R. Yang, *Nat. Photonics* **2016**, *10*, 699.
- [12] M. J. Yuan, L. N. Quan, R. Comin, G. Walters, R. Sabatini, O. Voznyy, S. Hoogland, Y. B. Zhao, E. M. Beauregard, P. Kanjanaboos, Z. H. Lu, D. H. Kim, E. H. Sargent, *Nat. Nanotechnol.* **2016**, *11*, 872.
- [13] Z. G. Xiao, R. A. Kerner, L. F. Zhao, N. L. Tran, K. M. Lee, T. W. Koh, G. D. Scholes, B. P. Rand, *Nat. Photonics* **2017**, *11*, 108.
- [14] H. Tsai, W. Nie, J.-C. Blancon, C. C. Stoumpos, R. Asadpour, B. Harutyunyan, A. J. Neukirch, R. Verduzco, J. J. Crochet, S. Tretiak, *Nature* **2016**, *536*, 312.
- [15] D. H. Cao, C. C. Stoumpos, O. K. Farha, J. T. Hupp, M. G. Kanatzidis, *J. Am. Chem. Soc.* **2015**, *137*, 7843.
- [16] X. L. Yang, X. W. Zhang, J. X. Deng, Z. M. Chu, Q. Jiang, J. H. Meng, P. Y. Wang, L. Q. Zhang, Z. G. Yin, J. B. You, *Nat. Commun.* **2018**, *9*, 8.
- [17] L. N. Quan, Y. B. A. Zhao, F. P. G. de Arquer, R. Sabatini, G. Walters, O. Voznyy, R. Comin, Y. Y. Li, J. Z. Fan, H. R. Tan, J. Pan, M. J. Yuan, O. M. Bakr, Z. H. Lu, D. H. Kim, E. H. Sargent, *Nano Lett.* **2017**, *17*, 3701.
- [18] J. Xing, Y. Zhao, M. Askerka, L. N. Quan, X. Gong, W. Zhao, J. Zhao, H. Tan, G. Long, L. Gao, Z. Yang, O. Voznyy, J. Tang, Z. H. Lu, Q. Xiong, E. H. Sargent, *Nat. Commun.* **2018**, *9*, 3541.
- [19] S. Yuan, Z. K. Wang, L. X. Xiao, C. F. Zhang, S. Y. Yang, B. B. Chen, H. T. Ge, Q. S. Tian, Y. Jin, L. S. Liao, *Adv. Mater.* **2019**, *31*, 1904319.
- [20] Y. Jin, Z. K. Wang, S. Yuan, Q. Wang, C. Qin, K. L. Wang, C. Dong, M. Li, Y. Liu, L. S. Liao, *Adv. Funct. Mater.* **2019**, *30*, 1908339.
- [21] F. Wang, Z. Wang, W. Sun, Z. Wang, Y. Bai, T. Hayat, A. Alsaedi, Z. Tan, *Small* **2020**, *16*, 2002940.
- [22] C. Wang, D. Han, J. Wang, Y. Yang, X. Liu, S. Huang, X. Zhang, S. Chang, K. Wu, H. Zhong, *Nat. Commun.* **2020**, *11*, 6428.
- [23] L. Kong, X. Zhang, Y. Li, H. Wang, Y. Jiang, S. Wang, M. You, C. Zhang, T. Zhang, S. V. Kershaw, W. Zheng, Y. Yang, Q. Lin, M. Yuan, A. L. Rogach, X. Yang, *Nat. Commun.* **2021**, *12*, 1246.
- [24] C. Sun, Y. Jiang, M. Cui, L. Qiao, J. Wei, Y. Huang, L. Zhang, T. He, S. Li, H.-Y. Hsu, C. Qin, R. Long, M. Yuan, *Nat. Commun.* **2021**, *12*, 2207.
- [25] S. Panuganti, L. V. Besteiro, E. S. Vasileiadou, J. M. Hoffman, A. O. Govorov, S. K. Gray, M. G. Kanatzidis, R. D. Schaller, *J. Am. Chem. Soc.* **2021**, *143*, 4244.
- [26] Z. Ren, J. Yu, Z. Qin, J. Wang, J. Sun, C. C. S. Chan, S. Ding, K. Wang, R. Chen, K. S. Wong, X. Lu, W. J. Yin, W. C. H. Choy, *Adv. Mater.* **2021**, *33*, 2005570.
- [27] Y. Shen, K. C. Shen, Y. Q. Li, M. Guo, J. Wang, Y. Ye, F. M. Xie, H. Ren, X. Gao, F. Song, J. X. Tang, *Adv. Funct. Mater.* **2020**, *31*, 2006736.
- [28] M. Abdi-Jalebi, Z. Andaji-Garmaroudi, S. Cacovich, C. Stavarakas, B. Philippe, J. M. Richter, M. Alsari, E. P. Booker, E. M. Hutter, A. J. Pearson, *Nature* **2018**, *555*, 497.
- [29] F. Yang, H. Chen, R. Zhang, X. Liu, W. Zhang, J. Zhang, F. Gao, L. Wang, *Adv. Funct. Mater.* **2020**, *30*, 1908760.
- [30] Y. Dong, Y. K. Wang, F. Yuan, A. Johnston, Y. Liu, D. Ma, M. J. Choi, B. Chen, M. Chekini, S. W. Baek, L. K. Sagar, J. Fan, Y. Hou, M. Wu, S. Lee, B. Sun, S. Hoogland, R. Quintero-Bermudez, H. Ebe, P. Todorovic, F. Dinic, P. Li, H. T. Kung, M. I. Saidaminov, E. Kumacheva, E. Spiecker, L. S. Liao, O. Voznyy, Z. H. Lu, E. H. Sargent, *Nat. Nanotechnol.* **2020**, *15*, 668.
- [31] T. Wu, J. Li, Y. Zou, H. Xu, K. Wen, S. Wan, S. Bai, T. Song, J. A. McLeod, S. Duhm, F. Gao, B. Sun, *Angew. Chem., Int. Ed.* **2019**, *59*, 4099.
- [32] C. Wu, T. Wu, Y. Yang, J. A. McLeod, Y. Wang, Y. Zou, T. Zhai, J. Li, M. Ban, T. Song, X. Gao, S. Duhm, H. Sirringhaus, B. Sun, *ACS Nano* **2019**, *13*, 1645.
- [33] H. Cho, S.-H. Jeong, M.-H. Park, Y.-H. Kim, C. Wolf, C.-L. Lee, J. H. Heo, A. Sadhanala, N. Myoung, S. Yoo, *Science* **2015**, *350*, 1222.
- [34] S. Lee, D. B. Kim, I. Hamilton, M. Daboczi, Y. S. Nam, B. R. Lee, B. Zhao, C. H. Jang, R. H. Friend, J. S. Kim, *Adv. Sci.* **2018**, *5*, 1801350.
- [35] N. Zhou, Y. Shen, L. Li, S. Tan, N. Liu, G. Zheng, Q. Chen, H. Zhou, *J. Am. Chem. Soc.* **2018**, *140*, 459.
- [36] L. Meng, E. P. Yao, Z. Hong, H. Chen, P. Sun, Z. Yang, G. Li, Y. Yang, *Adv. Mater.* **2017**, *29*, 1603826.
- [37] S. Lee, D. B. Kim, I. Hamilton, M. Daboczi, Y. S. Nam, B. R. Lee, B. Zhao, C. H. Jang, R. H. Friend, J. S. Kim, M. H. Song, *Adv. Sci.* **2018**, *5*, 1801350.
- [38] M. Yu, C. Yi, N. Wang, L. Zhang, R. Zou, Y. Tong, H. Chen, Y. Cao, Y. He, Y. Wang, M. Xu, Y. Liu, Y. Jin, W. Huang, J. Wang, *Adv. Opt. Mater.* **2018**, *7*, 1801575.
- [39] D. Han, M. Imran, M. Zhang, S. Chang, X. G. Wu, X. Zhang, J. Tang, M. Wang, S. Ali, X. Li, G. Yu, J. Han, L. Wang, B. Zou, H. Zhong, *ACS Nano* **2018**, *12*, 8808.
- [40] G. Zheng, C. Zhu, J. Ma, X. Zhang, G. Tang, R. Li, Y. Chen, L. Li, J. Hu, J. Hong, Q. Chen, X. Gao, H. Zhou, *Nat. Commun.* **2018**, *9*, 2793.
- [41] Z. Xu, Z. Liu, N. Li, G. Tang, G. Zheng, C. Zhu, Y. Chen, L. Wang, Y. Huang, L. Li, N. Zhou, J. Hong, Q. Chen, H. Zhou, *Adv. Mater.* **2019**, *31*, 1900390.
- [42] R. Quintero-Bermudez, A. Gold-Parker, A. H. Proppe, R. Munir, Z. Yang, S. O. Kelley, A. Amassian, M. F. Toney, E. H. Sargent, *Nat. Mater.* **2018**, *17*, 900.
- [43] Y. Jiang, M. Cui, S. Li, C. Sun, Y. Huang, J. Wei, L. Zhang, M. Lv, C. Qin, Y. Liu, M. Yuan, *Nat. Commun.* **2021**, *12*, 336.
- [44] Z. Yuan, Y. Miao, Z. Hu, W. Xu, C. Kuang, K. Pan, P. Liu, J. Lai, B. Sun, J. Wang, S. Bai, F. Gao, *Nat. Commun.* **2019**, *10*, 2818.
- [45] Y. H. Jia, S. Neutzner, Y. Zhou, M. Yang, J. M. F. Tapia, N. Li, H. Yu, J. Cao, J. P. Wang, A. Petrozza, *Adv. Funct. Mater.* **2020**, *30*, 1906875.
- [46] S. Tan, N. Zhou, Y. Chen, L. Li, G. Liu, P. Liu, C. Zhu, J. Lu, W. Sun, Q. Chen, H. Zhou, *Adv. Energy Mater.* **2018**, *9*, 1803024.
- [47] N. Zhou, B. Huang, M. Sun, Y. Zhang, L. Li, Y. Lun, X. Wang, J. Hong, Q. Chen, H. Zhou, *Adv. Energy Mater.* **2019**, *10*, 1901566.
- [48] Z. Wang, F. Wang, B. Zhao, S. Qu, T. Hayat, A. Alsaedi, L. Sui, K. Yuan, J. Zhang, Z. Wei, Z. A. Tan, *J. Phys. Chem. Lett.* **2020**, *11*, 1120.
- [49] P. Pang, G. Jin, C. Liang, B. Wang, W. Xiang, D. Zhang, J. Xu, W. Hong, Z. Xiao, L. Wang, G. Xing, J. Chen, D. Ma, *ACS Nano* **2020**, *14*, 11420.

- [50] L. N. a Quan, D. Ma, Y. Zhao, O. Voznyy, H. Yuan, E. Bladt, J. Pan, F. P. García de Arquer, R. Sabatini, Z. Piontkowski, A.-H. Emwas, P. Todorović, R. Quintero-Bermudez, G. Walters, J. Z. Fan, M. Liu, H. Tan, M. I. Saidaminov, L. Gao, Y. Li, D. H. Anjum, N. Wei, J. Tang, D. W. McCamant, M. B. J. Roeffaers, S. Bals, J. Hofkens, O. M. Bakr, Z.-H. Lu, E. H. Sargent, *Nat. Commun.* **2020**, *11*, 2186.
- [51] L. Xu, J. Li, B. Cai, J. Song, F. Zhang, T. Fang, H. Zeng, *Nat. Commun.* **2020**, *11*, 3902.
- [52] N. Li, L. Song, Y. Jia, Y. Dong, F. Xie, L. Wang, S. Tao, N. Zhao, *Adv. Mater.* **2020**, *32*, 1907786.
- [53] Y. Guo, Y. Jia, N. Li, M. Chen, S. Hu, C. Liu, N. Zhao, *Adv. Funct. Mater.* **2020**, *30*, 1910464.
- [54] Y. Guo, S. Apergi, N. Li, M. Chen, C. Yin, Z. Yuan, F. Gao, F. Xie, G. Brocks, S. Tao, N. Zhao, *Nat. Commun.* **2021**, *12*, 644.
- [55] L. Zhao, K. Roh, S. Kacmoli, K. Al Kurdi, S. Jhulki, S. Barlow, S. R. Marder, C. Gmachl, B. P. Rand, *Adv. Mater.* **2020**, *32*, 2000752.